A study on the reproducibility of counting vesicles in volcanic rocks

Don R. Baker[1,2], Margherita Polacci[3], and Alexandra LaRue[1]
[1]*Department of Earth and Planetary Sciences, McGill University, 3450 rue University, Montreal, Quebec H3A 2A7, Canada*
[2]*Microfluorescence Beamline Project, Sincrotrone Trieste S.C.p.A., S.S. 14, Km 163, 5 in Area Science Park, 34012 Basovizza (Trieste), Italy*
[3]*Istituto Nazionale di Geofisica e Vulcanologia, sezione di Pisa, via della Faggiola 32, 56126 Pisa, Italy*

ABSTRACT

Vesicle size distributions in two and three dimensions of two samples were independently measured by three different researchers to investigate whether or not such measurements are reproducible. Additionally, two different software programs were used to measure the three-dimensional vesicle size distributions: the 3D Object Counter plugin for ImageJ and Blob3D. Manual thresholding by each of the authors produced similar results for both samples using both programs; however, use of the automatic, maximum entropy technique for thresholding produced measurably different results because it did not discriminate between vesicles and plagioclase crystals in one case and between vesicles and some cracks in another. Use of asymmetric erosion and dilation processes on the images is shown to affect the vesicle size distribution, but it does not have a significant effect on the power-law exponent that describes intermediate-sized vesicles or on the vesicle number density in these samples. However, such a technique is not recommended.

INTRODUCTION

Since the time that humans first mined the Earth for materials, geologists have been accustomed to the need to understand the three-dimensional (3D) distribution of rocks and minerals in the Earth; a field geologist faced with an outcrop will almost certainly begin with a measurement of the strike and dip of any obvious strata. However, when a geologist must analyze a hand sample or a thin section, any complete description of object shapes and size distributions in 3D becomes almost impossible. Instead, in most cases the geologist can only present a two-dimensional (2D) description with inferences concerning the third dimension. However, in order to determine accurately the size distribution and the spatial orientations of objects in a sample, some form of 3D description is a necessity.

In the past centuries, geologists have used serial sectioning to provide 3D images of samples. A 2D section of a sample can be analyzed, and then the sample is ground or sliced, and the next 2D section is analyzed (for recent applications of this technique, see Mock and Jerram, 2005; and Duchêne et al., 2008). Using this time-consuming process, a suite of 2D images can be obtained and combined to yield the 3D structure. With this technique, the 3D orientations and size distributions can be completely determined to a resolution equivalent to that of the thickness of the sections. However, the laborious nature of this technique restricts the number of samples to which it can be applied, and thus the question of statistical representation must be raised.

Instead, most studies have relied upon 2D imaging of samples, often in standard thin sections, in order to analyze as many samples as possible and create a more statistically reliable set of measures (c.f. Cashman and Mangan, 1994, and references therein). Many studies have considered the 2D distributions and orientations to be accurate approximations to the real, 3D, ones (e.g., Lautze and Houghton, 2007).

Rigorous mathematical techniques and computer programs have been developed for the conversion of 2D size distributions into 3D ones (e.g., Cashman and Mangan, 1994; Gaonac'h et al., 1996a, 1996b, 2005; Sahagian and Proussevitch, 1998; Higgins, 2006; Shea et al., 2010), albeit with many limitations (Russ, 2002, p. 471–473). Commonly, one of the limitations of most of these techniques is that the shapes of all objects under investigation must be the same, and another is that they must be topologically convex; i.e., all tangents to the surface must not intersect the object at any other point. This requirement cannot be guaranteed for objects in many geological samples, and thus in some cases these techniques of converting from 2D to 3D are certain to fail. Although 2D imaging remains an important tool for geologists, and we have no intention of denigrating its importance in the study of rocks, 3D imaging must be performed to understand completely the textures of many samples (e.g., Gualda, 2006).

In this contribution, we compare 2D and 3D measures of vesicles in two different case studies of samples imaged by X-ray microtomography. Only rarely have similar studies comparing 2D and 3D measurements been performed in the past (e.g., Jerram et al., 2009). In particular, we concentrate on investigating the reproducibility of measuring cumulative vesicle size distributions in 2D and 3D by comparing the results of three researchers who were provided with identical tomograms of each sample and told to measure the vesicle size distribution using the software described below. No other instructions were provided. Only if we can demonstrate acceptable reproducibility can we rely on the results of this type of image analysis and make a meaningful comparison of the results of one researcher with another.

We also compare the results of two different software packages against each other. We, like most scientists, are not accomplished writers of computer software; thus we are dependent upon others to provide us with some of the fundamental tools for our analysis. However, we need to evaluate the software available and compare the results of different programs in order to find the software that provides the most accurate and reliable results for our studies.

As will be demonstrated, in most cases the results found by the researchers were similar to one another and demonstrate reproducibility. However, the techniques used by one of the authors produced 3D results with different bubble sizes than found by the other two authors, but the exponent of the power-law distribution found by these techniques was still similar to that found by the other authors.

Geosphere; February 2011; v. 7; no. 1; p. 70–78; doi: 10.1130/GES00553.1; 8 figures; 2 tables; 2 animations; 3 supplemental figures.

TECHNIQUES

The Measures

Two samples were chosen for the measurement of the cumulative vesicle size distribution (see Hergarten, 2002; Baker et al., 2006). If the cumulative size distribution of a set of objects is described by a power law, the exponent of the power law can be a characteristic measure of self-similar (e.g., fractal) objects (Hergarten, 2002). The cumulative vesicle size distribution is a convenient reference against which to compare our measurements because theory predicts that the distribution of vesicles formed by gas exsolution from a melt should be described by a power law. However, there are multiple theories that each predict a power-law exponent near 1 (Gaonac'h et al., 1996a, 1996b, 2005; Blower et al., 2002; Lovejoy et al., 2004; Baker et al., 2006), and some vesicle size distributions are known to display power-law exponents measurably different than 1 (e.g., Polacci et al., 2009). Despite the ambiguity concerning the origin of a power-law exponent of 1, we can compare our size distribution measurements to this expected value and use it as a reference in this study. Additionally, measuring the cumulative vesicle size distribution provides a reliable way to compare the 2D and 3D measurements of these vesicles (Gaonac'h et al., 1996a, 1996b, 2005).

The Samples

Two samples were chosen in order to represent end members in terms of ease of vesicle counting. (Tagged Image File Format [TIFF] image stacks of the samples are included with this paper as Supplemental Figures 1[1], 2[2], and 3[3].) We cannot avoid some subjectivity in our definition of samples as "easy" and "difficult" for the counting of vesicles, but our choices are based upon the authors' experience in the counting of more than one hundred samples. Both samples are similar, however, in that the vesicle shapes are not simple spheres (convex objects) as shown in Animations 1 and 2. Therefore, application of the elegant procedures to convert the 2D size distributions of convex objects to 3D size distributions will not work (e.g., Sahagian and Proussevitch, 1998).

The easy sample was a natural basaltic scoria from Stromboli volcano, Aeolian Islands, Italy, previously studied by Polacci et al. (2009). This sample is dominated by one, large vesicle with a complex shape, but it contains many moderate-sized vesicles (50–250 μm radius) that are spherical to subspherical in shape (Animation 1). The vesicles in this sample are obvious and easily distinguished from the rock around them because of their shapes and the large contrast between the rock and the air in the vesicles.

The difficult sample was a synthetic rhyolitic foam created in the laboratory by the heating of a hydrated rhyolitic glass following the techniques of Bai et al. (2008). The duration of the experiment was too short for the melt to relax, and the vesicles in this sample are small and far from spherical; additionally many cracks are present (Animation 2). The vesicles in this sample are much more difficult to distinguish from the glass around them because of their small size, their nonspherical shape, and the small density contrast between the vesicles and the glass in the images. These properties create a particular challenge to the researcher when trying to decide if two vesicles are touching, yet separate, or partially coalesced.

X-ray Microtomography Techniques

The Stromboli sample was imaged on the SYnchrotron Radiation for MEdical Physics (SYRMEP) beamline of the Elettra Synchrotron light source, Basovizza, Trieste, Italy. The sample was rotated 180°, and 900 images were acquired at one-fifth-degree intervals with a charge-coupled device (CCD) camera; the volume of each voxel was 9 × 9 × 9 μm^3. These images were reconstructed using the back-projection algorithm. Details of the experimental setup and of the reconstruction procedure can be found in Polacci et al. (2009). The volume of the analyzed tomogram was 14.128 mm^3.

The rhyolitic glass foam was imaged on the GeoSoilEnviroCARS (GSECARS) bending magnet beamline of the Advanced Photon Source, Argonne, Illinois, USA. A 20 keV incident X-ray beam was used, and the sample was rotated 180°, while 720 images were acquired at one-quarter-degree intervals with a CCD camera. The images have a voxel volume of 7.44 × 7.44 × 7.44 um^3. Reconstruction of the radiographs into the 3D tomogram was performed with the GridRec algorithm; further details of the experimental techniques are

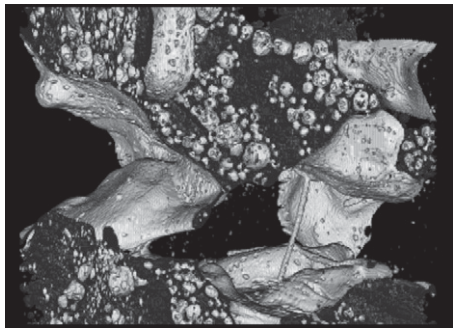

Animation 1. AVI video file of the three-dimensional tomographic reconstruction of sample Str240506b. The contrast has been adjusted to highlight the vesicle walls as light gray. Note the large interior bubble in this sample with the fine glass fibers that cross it. The large and nearly spherical vesicles in this sample are obvious and easily segmented from the glass and crystals that are also present. The volume of this sample is ~14 mm^3. This animation can be viewed using Windows Media Player or VLC or a similar media player. If you are viewing the PDF of this paper or reading it offline, please visit http://dx.doi.org/10.1130/GES00553.S4 or the full-text article on www.gsapubs.org to view Animation 1.

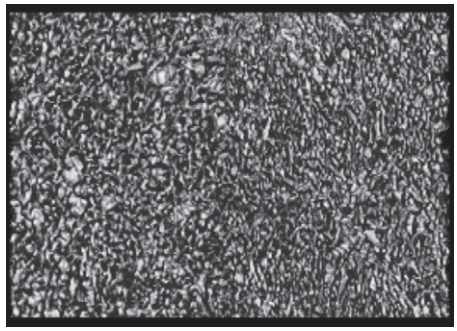

Animation 2. AVI video file of the three-dimensional tomographic reconstruction of sample ry4b. The contrast has been adjusted to highlight the vesicle walls as light gray. The small, convoluted vesicles are difficult to segment from the glass matrix of this sample. The volume of this sample is ~3.4 mm^3. This animation can be viewed using Windows Media Player or VLC or a similar media player. If you are viewing the PDF of this paper or reading it offline, please visit http://dx.doi.org/10.1130/GES00553.S5 or the full-text article on www.gsapubs.org to view Animation 2.

[1]Supplemental Figure 1. TIFF (Tagged Image File Format) image stack of Str240506b. If you are viewing the PDF of this paper or reading it offline, please visit http://dx.doi.org/10.1130/GES00553.S1 or the full-text article on www.gsapubs.org to view Supplemental Figure 1.

[2]Supplemental Figure 2. TIFF image stack of ry4b. If you are viewing the PDF of this paper or reading it offline, please visit http://dx.doi.org/10.1130/GES00553.S2 or the full-text article on www.gsapubs.org to view Supplemental Figure 2.

[3]Supplemental Figure 3. TIFF image stack of computer-generated sample. If you are viewing the PDF of this paper or reading it offline, please visit http://dx.doi.org/10.1130/GES00553.S3 or the full-text article on www.gsapubs.org to view Supplemental Figure 3.

provided in Robert et al. (2004) and Bai et al. (2008). The volume of tomogram of this sample that was analyzed depended upon the researcher, but only varied from 3.34 to 3.61 mm^3.

Software for Counting Vesicles

Two software packages were compared for counting vesicles in the samples: ImageJ (Rasband, 1997–2009; Abramoff et al., 2004) and Blob3D (Ketcham, 2005). The vesicles in the images were segmented from the glass and crystals by thresholding to convert the gray-scale images into the binary black and white images used for measuring vesicle numbers and sizes. In most cases the tomographic slices were manually thresholded by each of the three researchers who authored this contribution (identification numbers were randomly assigned to the researchers and do not correlate with the authorship order). Selected slices in the stack were observed and the threshold varied to produce the best differentiation between the vesicles and the remainder of the sample. Once the most suitable threshold was found, it was applied to all slices in the image stack simultaneously. In addition to manual thresholding, one researcher also applied the maximum entropy threshold method (Sahoo et al., 1988), using the Entropy Threshold plugin in ImageJ, before counting, in order to compare this automated thresholding technique to manual thresholding. After thresholding, the Analyze Particles subroutine in ImageJ was used for counting vesicles in the 2D slices, and the 3D Object Counter plugin was used for counting vesicles in the 3D volume. We found that the volumes produced by some versions of the 3D Object Counter plugin were incorrect by a factor that corresponded to the distance between the slices; therefore, volumes measured by this plugin were multiplied by the appropriate factor representing the distance between slices, either 9 or 7.44 µm. Blob3D was used only for the analysis of vesicles in the 3D volume, after the tomogram slices were thresholded in ImageJ.

A fundamental difference in use between the 3D Object Counter plugin and Blob3D is that the plugin only requires the user to threshold the images, and then it automatically counts all blobs within the selected thresholding range without further user input. Although Blob3D can be used in an automatic counting method similar to the 3D Object counter, it is our practice when using Blob3D to threshold the images and then investigate each blob individually to determine if it is an object of interest (in this case a vesicle) and whether two touching blobs should be separated into individual objects. The advantage of automatic counting is that the software can run unattended once it is started, as opposed to the manual procedures we follow with Blob3D, which require many hours of user time. The advantage of using Blob3D in its fully manual mode is that the user can carefully inspect the blobs and determine how to treat them, or reject them if they are artifacts.

RESULTS

Case Study 1: Natural Basaltic Scoria

2D Results

The tomographic image slices of the Stromboli scoria were manually thresholded by each of the three authors and counted in ImageJ (Fig. 1; Table 1). The total number of 2D vesicles counted in this sample varied from 21,000 to 33,000 (depending upon the researcher). These differences are above the expected counting uncertainty, which is proportional to the square root of the number of counted vesicles (see Baker et al., 2006). This number of vesicles greatly exceeds the minimum numbers of objects estimated to be necessary for a statistically representative sample, ~200–400 (Mock and Jerram, 2005; Gualda, 2006). The differences between the total number of counted vesicles by the different researchers reflect differences in the thresholding procedures used to separate the vesicles from the rest of the sample. However, because vesicle number densities typically vary by orders of magnitude between rocks (e.g., Polacci et al., 2009), the differences between the vesicle counts of the researchers are not considered significant.

The 2D vesicle areas between 10^3 and 10^5 μm^2 describe a power-law relationship with exponents, n_{2D}, between 0.77 and 0.79 (Fig. 1; Table 1). The uncertainties in these and subsequent power-law exponents are less than 0.2, as discussed in Baker et al. (2006). The vesicle number density, defined by the intersection of each distribution with the *y*-axis, found by the different authors varies from 10 to 20 vesicles per mm^2, and the maximum vesicle area is less than 5×10^6 μm^2 (Table 1).

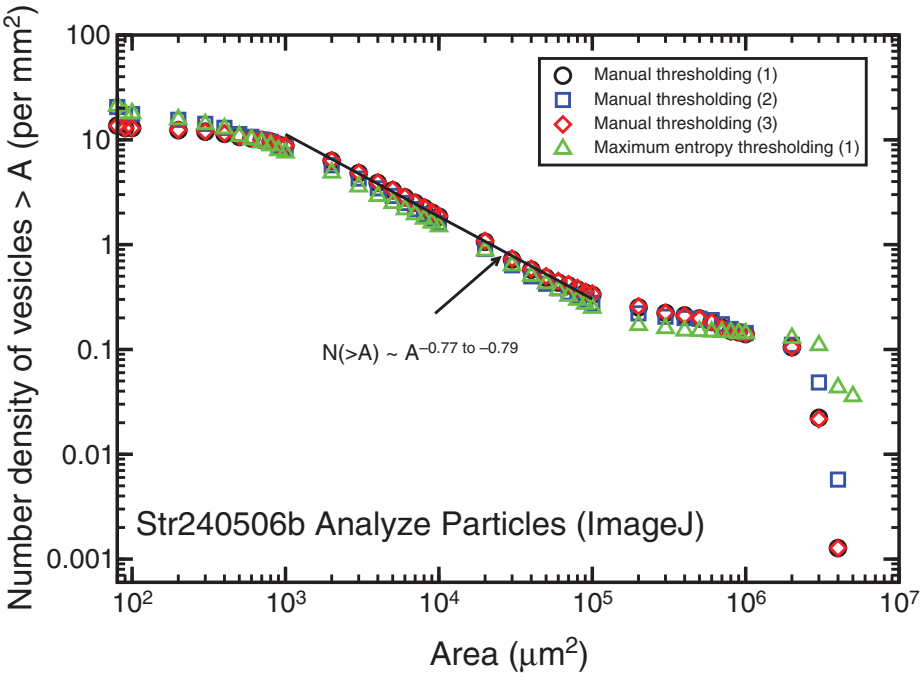

Figure 1. Cumulative two-dimensional vesicle area distribution for Str240506b as measured using the Analyze Particles routine in ImageJ. The legend for this and for subsequent plots of the cumulative vesicle size distributions indicates the technique used to threshold the image and separate the vesicles from the rest of the sample followed by a number in parentheses that was randomly assigned to each of the three authors of the paper in order to indicate their different results. The uncertainty in the number of vesicles is proportional to the square root of the number of vesicles counted in this and subsequent cumulative vesicle size figures. This uncertainty is smaller than the size of the symbols for vesicles over most of the range of the figures, but increases for the smallest vesicles. In this and subsequent figures individual power-law fits to the data sets that overlap one with another are not displayed, but the range of power-law exponents is provided. The uncertainty in each power-law exponent is less than or equal to 0.2 (see Baker et al., 2006).

TABLE 1. VESICLE MEASUREMENTS FOR NATURAL BASALTIC AND ARTIFICIAL RHYOLITIC SAMPLES

Thresholding	Manual			Maximum entropy
Researcher	1	2	3	1
		Sample STR240506b		
Two-dimensional measurements				
Sample size (mm^2)	1569.7	1569.7	1569.7	1569.7
Threshold used	117	129	128	Not recorded
Number of vesicles	21435	32272	21357	33104
Vesicle density (per mm^2)	13.65	20.56	13.72	21.09
Maximum vesicle (mm^2)	4.52	4.86	4.47	5.80
Porosity (%)	49.3	51.2	49.6	59.3
Power-law exponent	0.79	0.79	0.78	0.77
Three-dimensional measurements				
Sample size (mm^3)	14.128	14.128	14.128	14.128
ImageJ 3D object counter				
Number of vesicles	1115	2314	335	783
Vesicle density (per mm^3)	78.92	163.8	23.71	55.42
Maximum vesicle (mm^3)	6.84	7.10	7.18	8.35
Porosity (%)	49.2	51.1	50.8	59.2
Power-law exponent	0.96	1.06	1.55	0.98
Blob3D				
Number of vesicles	1687	4117	1073	2112
Vesicle density (per mm^3)	119.4	291.4	75.95	129.5
Maximum vesicle (mm^3)	6.81	7.04	4.67	8.30
Porosity (%)	49.2	51.1	38.2	59.2
Power-law exponent	0.90	1.00	0.95	1.02
		Sample ry4b		
Two-dimensional measurements				
Sample size (mm^2)	451.6	449.0	486.2	451.6
Threshold used	129	128	128	Not recorded
Number of vesicles	73736	84958	73821	76524
Vesicle density (per mm^2)	163.3	189.2	151.8	169.5
Maximum vesicle (mm^2)	0.511	0.334	0.696	2.20
Porosity (%)	36.7	36.1	42.8	40.5
Power-law exponent	1.27	1.33	1.05	1.19
Three-dimensional measurements				
Sample size (mm^3)	3.36	3.34	3.62	3.36
ImageJ 3D object counter				
Number of vesicles	3300	403	402	1615
Vesicle density (per mm^3)	982.1	120.7	111.0	480.6
Maximum vesicle (mm^3)	1.20	1.20	1.49	1.35
Porosity (%)	35.9	36.2	41.1	40.4
Power-law exponent	1.92	1.75	1.83	1.81
Blob3D				
Number of vesicles	8047	3148	3453	2368
Vesicle density (per mm^3)	2394	942.5	953.9	704.8
Maximum vesicle (mm^3)	0.843	1.18	0.036	1.33
Porosity (%)	27.9	36.2	41.0	40.3
Power-law exponent	1.46	1.86	1.78	1.77

3D Results

The 3D results are almost as consistent as the 2D ones (Figs. 2 and 3; Table 1). The number of vesicles counted with the 3D Object counter varied from 300 to 4000, and the number counted manually with Blob3D ranged from 1100 to 4100. After manual or maximum entropy thresholding and application of the 3D Object Counter routine in ImageJ, each researcher found that a portion of the measured vesicle-volume distribution is described by a power law. The exponents of these power laws, n_{3D}, ranged from 0.96 to 1.55 (Table 1). Three of the four distributions describe power laws for vesicle volumes of ~10^4 to 10^6 μm^3, and one distribution describes a power law from 10^3 to 10^4 μm^3. Although all researchers measured the largest vesicle to be near 10^{10} μm^3, their second-largest vesicle varied from ~10^4 to 10^7 μm^3. The number density of vesicles varied by over a factor of 10, from 20 to 300 vesicles mm^{-3} (Fig. 2; Table 1); however, three out of the four densities fell between 20 and 80 vesicles mm^{-3}. The maximum entropy thresholding routine produced a much more distinctive curved, exponential tail to the power-law distribution than the manual thresholding done by the same researcher.

The 3D power-law exponents near 1 (Table 1) are only slightly greater than those calculated from the 2D exponent, $n_{3D} = 2n_{2D}/3 + 1/3$ (Gaonac'h et al., 1996a, 1996b). However, the exponent of 1.55 seen for one of the distributions is far too high to be consistent with the 2D power-law exponents measured on the same thresholded images.

Counting the vesicles in 3D with Blob3D produces much more consistent power-law distributions for the three researchers than using the 3D Object Counter plugin of ImageJ (Fig. 3). Researcher #3 modified their methods in Blob3D for this vesicle count by applying two erosion steps followed by one dilation step (see Russ, 2002, for a complete description of these processes) to the vesicles. Based upon a series of empirical studies investigating the best techniques for separating and segmenting vesicles, researcher #3 found that this asymmetric combination of two erosions and one dilation produced a more accurate separation of impinging vesicles than any other technique they tried. However, this technique results in reduced vesicle volumes because only one dilation step follows the two erosion steps, and, as documented below, this procedure creates distributions that are significantly different from the others.

In this sample, all 3D distributions display power laws with exponents near one (Table 1), and therefore consistent with the 2D distributions; two out of the three have power-law distributions between ~10^4 and 10^6 μm^3, whereas one power-law distribution is only seen between 10^4 and 10^5 μm^3 and another between 10^5 and 10^8 μm^3. The maximum vesicle in each distribution is ~10^{10} μm^3, the same volume as measured using ImageJ. The maximum entropy thresholding technique also yields a more exponential-like distribution than the manually thresholded examples, as previously seen when using the 3D Object counter plugin for ImageJ. The measured vesiculation density in these distributions varies from 80 to 300 vesicles mm^{-3} (Table 1). The distribution with the lowest vesicle number density and the power-law distribution from 10^5 to 10^8 μm^3 is the one measured by researcher #3, who performed the asymmetric erode and dilate processes before counting the vesicles; these processes also result in a lower porosity than measured by the other techniques (Table 1).

Case Study 2: The Synthetic Rhyolitic Glass Foam

2D Results

The number of 2D vesicles counted in this sample ranged from 70,000 to 90,000. This variation is attributed to the slightly different volumes investigated by each researcher. The vesicle size distributions determined by each author for this sample are almost identical at vesicle areas up to ~3×10^5 μm^2, but differ slightly at larger areas (Fig. 4; Table 1). In particular, the maximum entropy thresholded results produced a vesicle

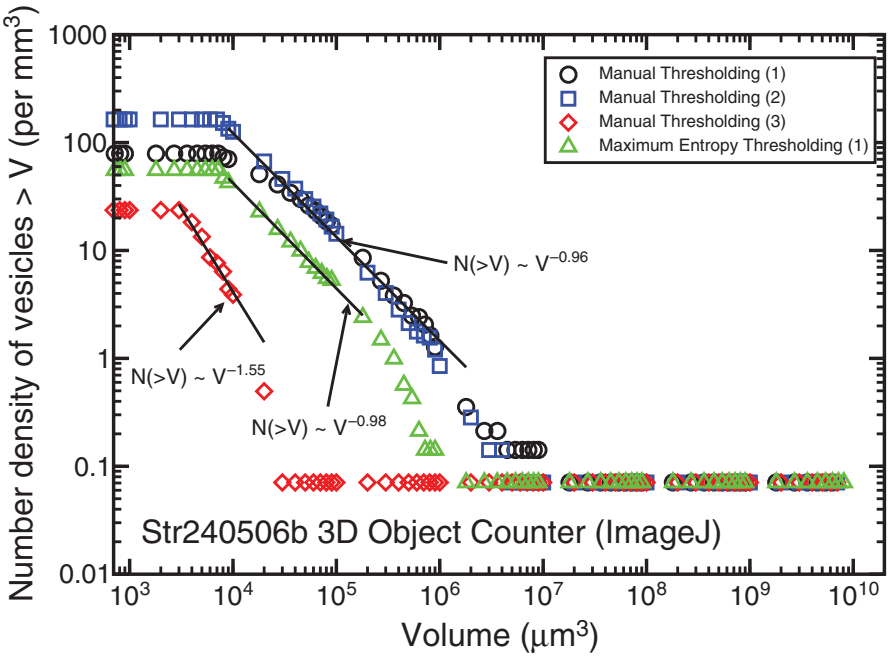

Figure 2. Cumulative three-dimensional (3D) vesicle-volume distribution for Str240506b determined using the 3D Object Counter plugin in ImageJ.

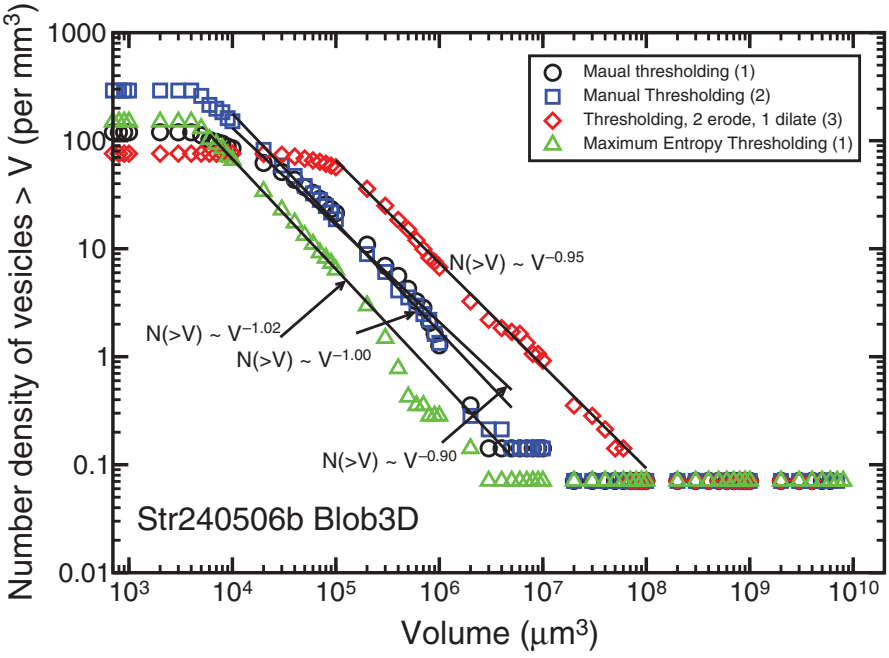

Figure 3. Cumulative three-dimensional (3D) vesicle-volume distribution for Str240506b found with Blob3D.

approximately two to six times larger than the largest found by any other thresholding technique used by the authors.

Fitting a power-law function to these 2D data produced exponents that varied from 1.05 to 1.33 for vesicles with areas between 10^3 and 10^5 μm^2 (Fig. 4; Table 1). These exponents are almost within uncertainty of each other, but appear to be larger than those measured for the Stromboli scoria. Despite the larger vesicles found in the maximum entropy thresholded results, the power-law exponent for this distribution is similar to those of the other results. However, the vesicle size distributions all display concavity downward for areas between 10^4 and 10^6 μm^2, possibly indicative of an evolution from a power-law distribution to an exponential one (Baker et al., 2006; Bai et al., 2008).

3D Results

Based upon counting 400–3500 vesicles, the results of using the 3D Object Counter plugin obtained by the researchers are in substantial agreement with each other (Fig. 5; Table 1), with the exception of two data sets that display vesicle number densities near 100 and two (both obtained by researcher #1) that have vesicle number densities of 500–600. All researchers found the maximum vesicle to be slightly smaller than 10^9 μm^3 and the second-largest to be ~7×10^4 μm^3. The 3D vesicle-volume distributions display power-law distributions with exponents that vary from 1.75 to 1.92 (Table 1), values substantially higher than calculated from the 2D measurements. These vesicle-volume distributions also display the downward curvature seen in the 2D vesicle area distributions (Fig. 4).

The 3D results from counting 2400–3500 vesicles with the Blob3D software are very similar to those of the 3D Object Counter, with the exception of the images to which researcher #3 applied two erode and one dilate processes in Blob3D (Fig. 6). The maximum vesicle found with this software is ~10^9 μm^3, and the second-largest vesicle varies from 10^5 to 10^7 μm^3. The measured vesicle number density is tightly constrained between 700 and 900 (Table 1). Although the application of the asymmetric erosion and dilation processes significantly affects the vesicle-volume distribution, the power-law exponents found by the researchers vary between 1.46 and 1.86 and are not significantly different from those obtained with the 3D Object Counter plugin (Table 1).

DISCUSSION

Reproducibility of Thresholding

Our first concern when starting this study was that different researchers would threshold the images at different levels and produce significantly different vesicle size distributions and vesicle number densities; thankfully this fear was unfounded. The close similarity of all 2D results for each sample (Figs. 1 and 4) demonstrate that all researchers chose thresholding levels close to each other and close to that calculated by the maximum entropy thresholding plugin in ImageJ.

The maximum entropy thresholding plugin produces larger vesicles that are more abundant

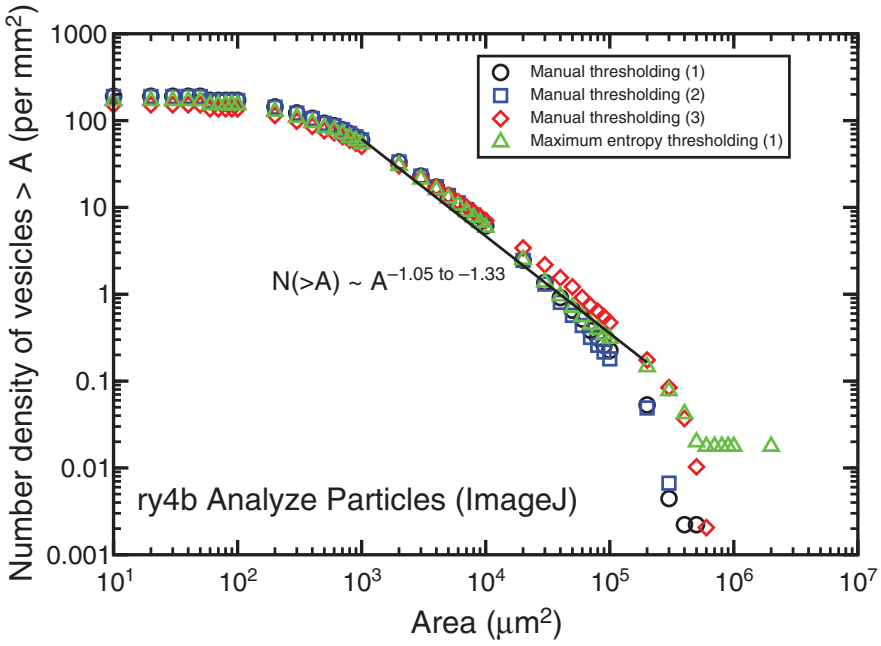

Figure 4. Cumulative two-dimensional vesicle area distribution for ry4b as measured by the Analyze Particles routine in ImageJ.

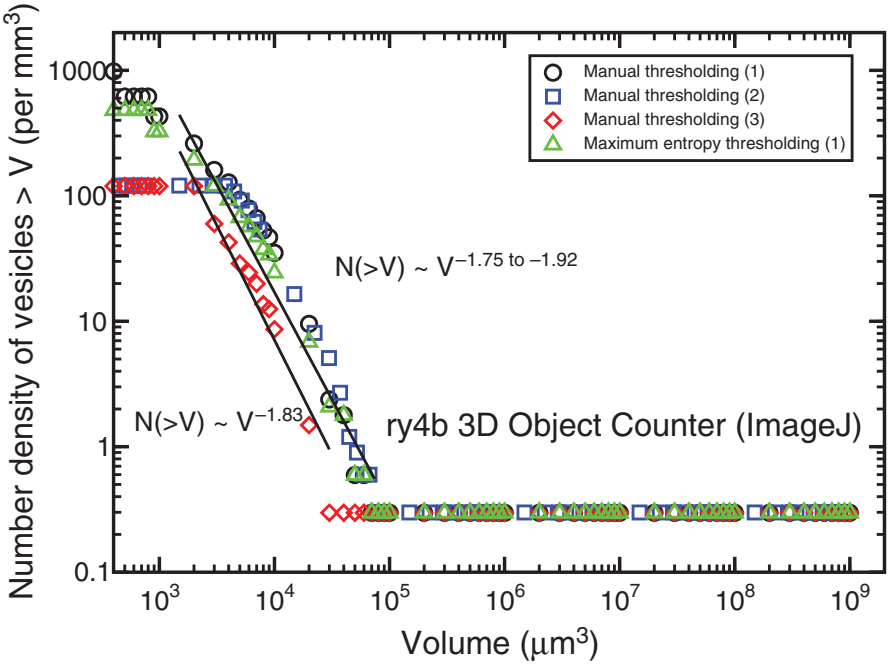

Figure 5. Cumulative three-dimensional (3D) vesicle-volume distribution for ry4b counted using the 3D Object Counter plugin in ImageJ.

than found using the manual thresholding performed by the authors. For Str240506b, the difference in vesicle size is small, ~4 × 10^6 µm² versus ~5 × 10^6 µm², but with an abundance of 0.04 per mm² as opposed to an abundance found by manual thresholding between 0.001 and 0.006 per mm². In ry4b, the largest vesicle determined by the maximum entropy thresholding is ~2 × 10^6 µm², compared to manual thresholding, which found maximum vesicle sizes between ~3 and 6 × 10^5 µm². The abundance of the largest vesicle in ry4b varied by a factor of 10, from 0.002 per mm² for the manually thresholded data to 0.02 per mm², for the maximum entropy thresholded measurements.

The discrepancy between the maximum entropy thresholded results and the other results for sample Str240506b is caused by the maximum entropy plugin misidentifying plagioclase crystals as vesicles (Fig. 7). Because most of the plagioclase crystals in this sample are large, they artificially increase the size and number of the largest vesicles. For sample ry4b, the difference between manual and maximum entropy thresholding is due to the eight vesicles of size 2 × 10^6 µm² that were counted in the maximum entropy thresholded tomogram slices. These vesicles appear to be expansion cracks that were not selected during manual thresholding. Thus, despite the advantage of eliminating subjective decisions made by humans that maximum entropy thresholding provides, the reproducibility demonstrated by the manually thresholded results demonstrates that this technique is the more reliable thresholding method of the two investigated.

3D Object Counter and Blob3D Results

Unlike the 2D results, the 3D results for each sample demonstrate variability at low vesicle volumes, but they converge at large volumes (Figs. 2, 3, 5, and 6). Despite these differences, the vesicle number densities vary by less than a factor of 10, and the 3D power-law exponents of all but one of the vesicle size distributions are similar for each sample. And, as seen in the 2D observations, the vesicle-volume distributions for Str240506b are better fit by a power law than the distributions measured for ry4b.

The porosity and power-law exponents calculated from results of the 3D Object Counter plugin used by the different researchers are consistent in all but one case (Figs. 2 and 5; Table 1). However, the number of vesicles counted can vary by approximately a factor of 7 (Table 1). These variations are attributed to minor differences in the thresholding used by the different researchers.

The vesicle size distributions measured with Blob3D are very similar to each other (Figs. 3 and 6; Table 1). The power-law exponent measured for each sample can be reproduced by the different researchers, with one exception. Significant differences in the vesicle-volume distributions are seen in the distributions measured after the application of two erosions and one dilation. This procedure results in the creation of more vesicles in the intermediate size ranges of ~10^5 to 10^8 µm³, but does not have a significant effect on the power-law exponent and only a

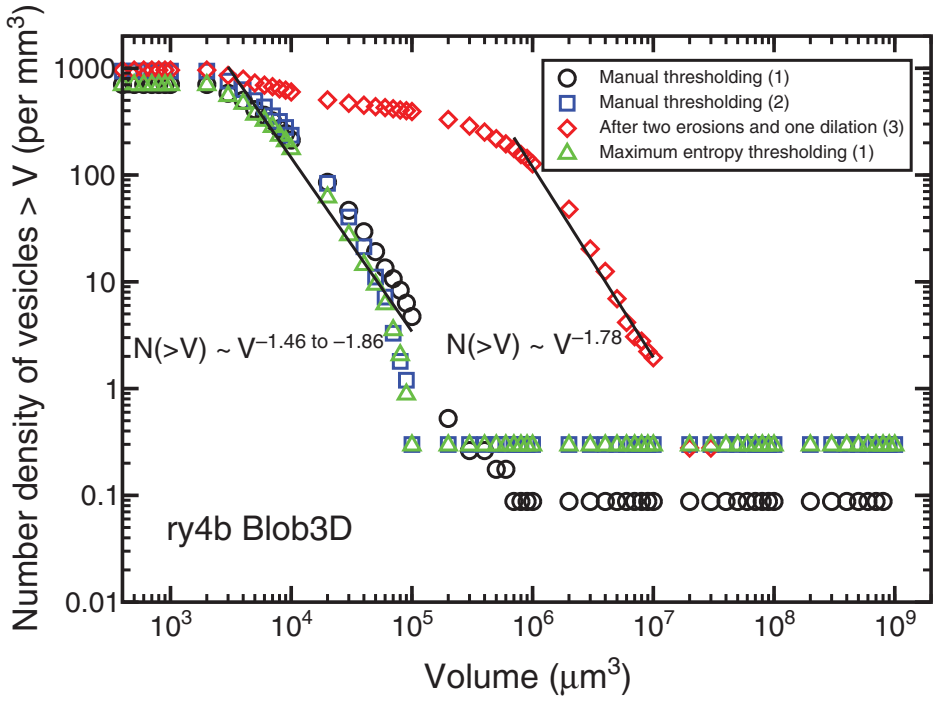

Figure 6. Cumulative three-dimensional (3D) vesicle-volume distribution for ry4b measured with Blob3D.

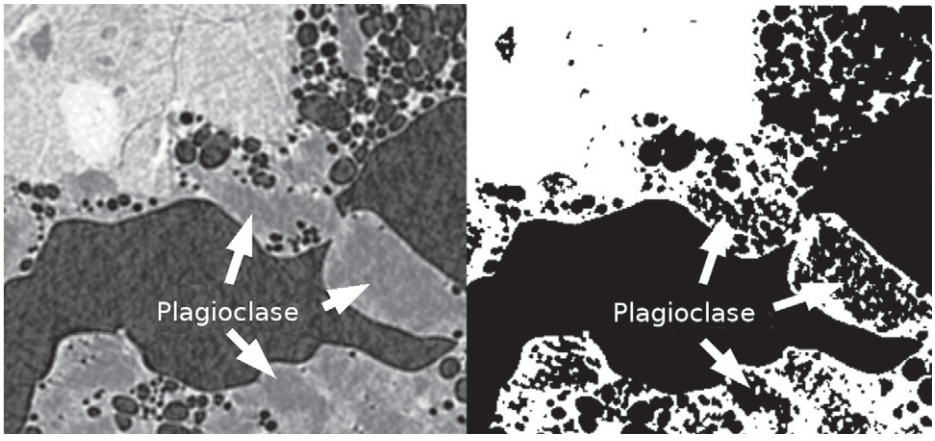

Figure 7. Slice 108 of Str240506b—before thresholding (left) and after thresholding using the maximum entropy algorithm in the ImageJ plugin. Note how the three example plagioclase crystals in the left-hand image are incorrectly separated out as vesicles in the right-hand image by the maximum entropy thresholding plugin.

small effect on the maximum measured vesicle volume in the sample (Table 1).

To test the effects of these erosion and dilation procedures, we created a synthetic data set using the continuum percolation program described in Baker et al. (2002). This program was modified to create spherical objects with a volume, V, a distribution proportional to $V^{-0.8}$, and a maximum radius of 11 voxels in a system of size 200 × 200 × 200 voxels. The results of the simulation were converted to a stack of binary TIFF images. These simulations have the advantage of eliminating the thresholding process; in this case, we know that the images created must represent the true vesicularity of this computer-generated sample. The vesicularity in this artificial tomogram was counted with the 3D Object Counter plugin in ImageJ and with the automated counting option in Blob3D, which allows the user to bypass inspection of each individual blob. The synthetic vesicles in the images were then eroded twice and dilated once and counted again in ImageJ and Blob3D. As shown in Figure 8, this procedure reduces the size of the largest vesicle from ~5 × 10^6 to 2 × 10^6 voxels (Table 2), but increases the number of vesicles in the medium size range significantly. Apparently, many narrow connections between parts of the largest vesicle are severed by the erosion and dilation process reducing its size and creating numerous smaller vesicles. This procedure significantly lowers the measured porosity, as also seen in the Str240506b sample (Table 1) counted by researcher #3.

The erosion and dilation process did not change the calculated power-law exponents of the vesicle-volume distributions (Fig. 8; Table 2) when counted using the 3D Object Counter Plugin. The power-law exponents from the 3D Object Counter plugin results are slightly higher than the value of the exponent used in the simulation, 0.9 versus 0.8, respectively. However, the exponent of 0.9 in the measurements is only seen at small vesicle volumes, less than ~8 voxels in volume (Fig. 8), due to the fact that the simulations do not take into account the volume of two overlapping vesicles. Because Blob3D did not consider any vesicles smaller than 6 voxels, the power-law segment of the distribution with an exponent of 0.9 is not seen in Figure 8. The effect of ignoring the combined volumes of two (or more) coalesced vesicles becomes even greater for larger vesicles. The power-law exponent measured for large vesicles in the original data set equals 2 when counted using the 3D Object Counter plugin and 1.8 when automatically counted using Blob3D (Fig. 8; Table 2). However, the asymmetric erosion and dilation procedure yields distributions with power laws of 0.9 when measured with either the 3D Object Counter plugin or Blob3D (Fig. 8; Table 2).

Comparison of Str240506b (Fig. 5; Table 1) and the simulation (Fig. 8; Table 2) shows that the effects of the asymmetric erosion and dilation procedure on the vesicle size distribution and power-law exponents are similar. Clearly, the application of erosion and dilation procedures to samples must be performed with caution, and it is only through experience that a researcher can determine if they produce a better measure than gray-scale thresholding. However, the asymmetric erosion and dilation procedure is not recommended for use.

The total vesicle number densities (Table 1 and the intercept of the distributions with the *y*-axis of the figures) display much less variation and tend to be higher when counted using Blob3D than when using the 3D Object Counter

TABLE 2. VESICLE MEASUREMENTS FOR COMPUTER-GENERATED SAMPLE

	Original sample	After two erosions and one dilation
ImageJ 3D object counter		
Number of vesicles	1786	1031
Maximum vesicle (voxels)	4.6188×10^6	1.6510×10^6
Porosity (%)	57.8	29.0
Power-law exponents	0.9, 2.0	0.9
Blob3D		
Number of vesicles	4836	1162
Maximum vesicle (voxels)	4.5130×10^6	2.1256×10^6
Porosity (%)	57.3	29.0
Power-law exponents	1.8	0.9

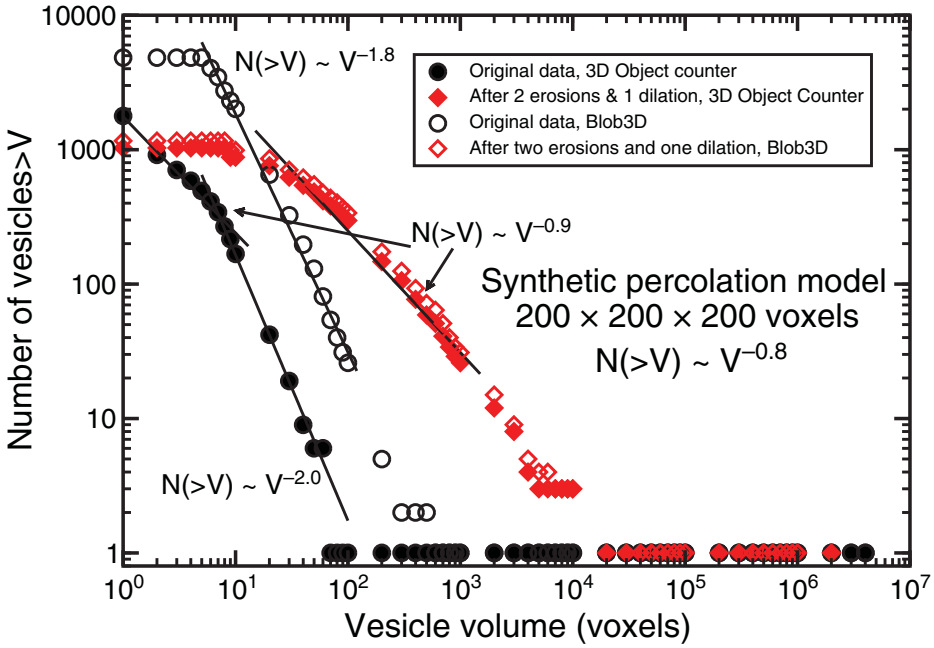

Figure 8. Comparison of vesicle size distributions from a synthetic data set. The data set was created with a vesicle-volume power-law exponent of 0.8 and analyzed with the 3D Object Counter plugin from ImageJ and with Blob3D set to count vesicles automatically. The sample was then subjected to two erosions and one dilation and recounted in the same manner as before. This erosion and dilation procedure results in reducing the volume of the largest vesicle and creating more vesicles in the medium size classes. Please see the text for further details.

plugin. The synthetic sample was also used to test this difference. Comparing the results of the two automated vesicle size distributions is enlightening (Fig. 8; Table 2). Despite the fact that Blob3D did not consider any vesicle smaller than six voxels, the number of vesicles that this software found was approximately three times that found by the 3D Object Counter.

Subjecting this computer-generated sample to the procedure of two erosions and one dilation before counting reveals that in this case Blob3D and the 3D Object Counter yield vesicle distributions within error of each other (Fig. 8; Table 2). This agreement demonstrates that the differences seen in the results of counting the original figures (Fig. 8; Table 2) are due to small vesicles and thin connections between large vesicles that are destroyed by the erosion and dilation procedure.

The measured variations seen in the vesicle number densities indicate that differences in this value of less than approximately a factor of 10 between samples may not be significant, but differences between vesicle number densities on the order of 25 or greater clearly exceed our counting uncertainty and reflect real variations in this measure.

The artifacts seen in the 2D vesicle area distributions that were thresholded with the maximum entropy method are not visible in the 3D distributions. However, in both samples, the maximum entropy thresholded distributions display an upper cutoff (i.e., downward deflection of the data set) of the power-law behavior at smaller volumes than the other distributions (best seen in Fig. 2 but present in the other figures). Thus, the maximum entropy thresholding technique does not produce 3D results as consistent as manual thresholding.

CONCLUSION

The ability of three researchers to manually threshold two vesicular samples and separate vesicles from other phases in the samples (glass and crystals) and produce similar results demonstrates that the subjectivity inherent in manual thresholding is insignificant (at least for the samples under investigation). Problems in separating vesicles from crystals and some cracks from vesicles were found using the maximum entropy automatic thresholding technique. We recommend that this technique, and most probably all other automatic thresholding techniques, be used with caution. We additionally identified problems with the asymmetric erosion and dilation technique. Even though this technique produced distributions with power-law exponents similar to those found using other segmentation procedures, the bubble sizes and number densities are measurably different than when counted with other procedures, and therefore this technique is not recommended.

The vesicle-volume distributions measured with the 3D Object Counter plugin of ImageJ and the Blob3D results are similar. However, Blob3D is our preferred software tool for measuring vesicle size distributions in volcanic rocks because its results are more reproducible when three researchers independently apply it to manually measure the vesicles in different samples. The superiority of Blob3D is due to the procedure we use of investigating each blob (vesicle, in this case) individually, which allows the rejection of thresholded objects that are not the phase of interest but may have been accidentally selected during the thresholding process and the separation of two touching, but not interconnected objects. Nevertheless, manual thresholding followed by use of the 3D Object Counter plugin or Blob3D in its automatic counting mode is an easy-to-use and rapid tool for the measurement of vesicle-volume distributions. Combining these techniques with a portable X-ray tomograph may make in situ, near real-time, measurements of vesicle size distributions possible, which could aid in the understanding of ongoing volcanic eruptions.

ACKNOWLEDGMENTS

Reviews by Guil Gualda, Richard Ketcham, and an anonymous reviewer helped improve and clarify this work. Some of the research herein described

was performed at GeoSoilEnviroCARS (Sector 13) of the Advanced Photon Source at Argonne National Laboratory with the help of Mark Rivers. GeoSoilEnviroCARS is supported by the National Science Foundation–Earth Sciences (EAR-0622171) and Department of Energy–Geosciences (DE-FG02-94ER14466). Use of the Advanced Photon Source was supported by the U.S. Department of Energy, Office of Science, Office of Basic Energy Sciences, under Contract No. DE-AC02-06CH11357. Other portions of this research were performed at Sincrotrone Trieste (Elettra) with the help of Lucia Mancini. Portions of this research were funded by a Natural Sciences and Engineering Research Council of Canada discovery grant to D.R.B.

REFERENCES CITED

Abramoff, M.D., Magelhaes, P.J., and Ram, S.J., 2004, Image Processing with ImageJ: Biophotonics International, v. 11, p. 36–42.

Bai, L., Baker, D.R., and Rivers, M., 2008, Experimental study of bubble growth in Stromboli basalt melts at 1 atmosphere: Earth and Planetary Science Letters, v. 267, p. 533–547, doi: 10.1016/j.epsl.2007.11.063.

Baker, D.R., Paul, G., Sreenivasan, S., and Stanley, H.E., 2002, The continuum percolation threshold for interpenetrating squares and cubes: Physical Review E: Statistical, Nonlinear, and Soft Matter Physics, v. 66, p. 046136.

Baker, D.R., Lang, P., Robert, G., Bergevin, J.-F., Allard, E., and Bai, L., 2006, Bubble growth in slightly supersaturated albite melt at constant pressure: Geochimica et Cosmochimica Acta, v. 70, p. 1821–1838, doi: 10.1016/j.gca.2006.01.011.

Blower, J.D., Keating, J.P., Mader, H.M., and Phillips, J.C., 2002, The evolution of bubble size distribution in volcanic eruptions: Journal of Volcanology and Geothermal Research, v. 120, p. 1–23, doi: 10.1016/S0377-0273(02)00404-3.

Cashman, K.V., and Mangan, M.T., 1994, Physical aspects of magmatic degassing: II. Constraints on vesiculation processes from textural studies of eruptive products, *in* Carroll M.R., and Holloway, J.R., eds., Volatiles in Magmas: Washington, D.C., Mineralogical Society of America, Reviews in Mineralogy, v. 30, p. 447–478.

Duchêne, S., Pupier, E., Le Carlier de Veslud, C., and Toplis, M.J., 2008, A 3D reconstruction of plagioclase crystals in a synthetic basalt: The American Mineralogist, v. 93, p. 893–901, doi: 10.2138/am.2008.2679.

Gaonac'h, H., Stix, J., and Lovejoy, S., 1996a, Scaling effects on vesicle shape, size, and heterogeneity of lavas from Mount Etna: Journal of Volcanology and Geothermal Research, v. 74, p. 131–153, doi: 10.1016/S0377-0273(96)00045-5.

Gaonac'h, H., Lovejoy, S., Stix, J., and Scherzter, D., 1996b, A scaling growth model for bubbles in basaltic lava flows: Earth and Planetary Science Letters, v. 139, p. 395–409.

Gaonac'h, H., Lovejoy, S., and Scherzter, D., 2005, Scaling vesicle distributions and volcanic eruptions: Bulletin of Volcanology, v. 67, p. 350–357, doi: 10.1007/s00445-004-0376-4.

Gualda, G.A.R., 2006, Crystal size distributions derived from 3D datasets: Sample size versus uncertainty: Journal of Petrology, v. 47, p. 1245–1254, doi: 10.1093/petrology/egl010.

Hergarten, S., 2002, Self-Organized Criticality in Earth Systems: Berlin, Springer, 272 p.

Higgins, M.D., 2006, Quantitative Textural Methods in Igneous and Metamorphic Petrology: Cambridge, Cambridge University Press, 276 p.

Jerram, D.A., Mock, A., Davis, G.R., Field, M., and Brown, R.J., 2009, 3D crystal size distributions: A case study on quantifying olivine populations in kimberlites: Lithos, v. 112, p. 223–235, doi: 10.1016/j.lithos.2009.05.042.

Ketcham, R.A., 2005, Computational methods for quantitative analysis of three-dimensional features in geological specimens: Geosphere, v. 1, p. 32–41, doi: 10.1130/GES00001.1.

Lautze, N.C., and Houghton, B.F., 2007, Linking variable explosion style and magma textures during 2002 at Stromboli volcano, Italy: Bulletin of Volcanology, v. 69, p. 445–460, doi: 10.1007/s00445-006-0086-1.

Lovejoy, S., Gaonac'h, H., and Schertzer, D., 2004, Bubble distributions and dynamics: The expansion-coalescence equation: Journal of Geophysical Research, v. 109, p. B11203, doi: 10.1029/2003JB002823.

Mock, A., and Jerram, D.A., 2005, Crystal size distributions (CSD) in three dimensions: Insights from the 3D reconstruction of a highly porphyritic rhyolite: Journal of Petrology, v. 46, p. 1525–1541, doi: 10.1093/petrology/egi024.

Polacci, M., Baker, D.R., Mancini, L., Favretto, S., and Hill, R.J., 2009, Vesiculation in magmas from Stromboli and implications for normal Strombolian activity and paroxysmal explosions in basaltic systems: Journal of Geophysical Research, v. 114, B01206, 14 p., doi: 10.1029/2008JB005672.

Rasband, W.S., 1997–2009, ImageJ: Bethesda, Maryland, USA, U.S. National Institutes of Health, http://rsb.info.nih.gov/ij/.

Robert, G., Baker, D.R., Rivers, M.L., Allard, E., and Larocque, J., 2004, Comparison of the bubble size distribution in silicate foams using 2-dimensional images and 3-dimensional X-ray microtomography, *in* Proceedings of SPIE, Developments in X-Ray Tomography IV, v. 5535, p. 505–514.

Russ, J.C., 2002, The Image Processing Handbook, 4th Edition: Boca Raton, CRC Press, 732 p.

Sahagian, D.L., and Proussevitch, A.A., 1998, 3D particle size distribution from 2D observations: Stereology for natural applications: Journal of Volcanology and Geothermal Research, v. 84, p. 173–196, doi: 10.1016/S0377-0273(98)00043-2.

Sahoo, P.K., Soltani, S., Wong, K.C., and Chen, Y.C., 1988, A survey of thresholding techniques: Computer Vision Graphics and Image Processing, v. 41, p. 233–260, doi: 10.1016/0734-189X(88)90022-9.

Shea, T., Houghton, B.F., Gurioli, L., Cashman, K.V., Hammer, J.E., and Hobden, B.J., 2010, Textural studies of vesicles in volcanic rocks: An integrated methodology: Journal of Volcanology and Geothermal Research, v. 190, p. 271–289, doi: 10.1016/j.jvolgeores.2009.12.003.

Manuscript Received 26 October 2009
Revised Manuscript Received 24 June 2010
Manuscript Accepted 19 September 2010